Thermodynamic Hydricity of a Ruthenium CO_2 Hydrogenation Catalyst Supported by a Rigid PNP Pincer

Published as part of JACS Au special issue "Advances in Small Molecule Activation Towards Sustainable Chemical Transformations".

Juwon Paik, Jong Hyeak Choe, Sudakar Padmanaban, Misook Seo, Chun-Jae Yoo, Heui Beom Lee,* and Yunho Lee*
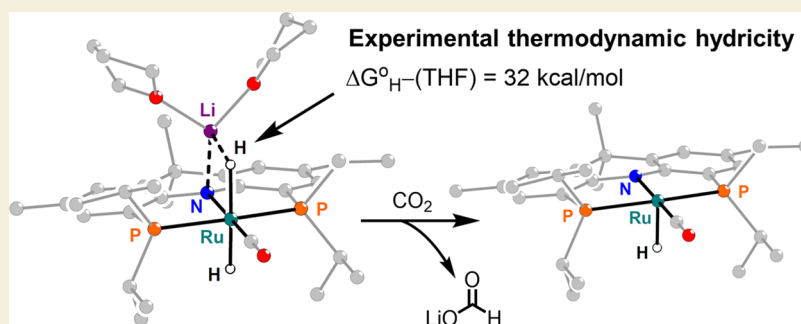
Read Online

ACCESS | Metrics & More | Article Recommendations | SI Supporting Information

Experimental thermodynamic hydricity
$\Delta G^o_{H^-}(THF) = 32$ kcal/mol

ABSTRACT: Ruthenium hydride complexes supported by pincer ligands play a crucial role in the catalytic hydrogenation of CO_2 to reduced C_1 chemicals such as formic acid and methanol. Toward a better understanding of their hydride transfer reactivity, knowledge of the underlying thermodynamic hydricity values is deemed critical, but relevant studies remain rare. Herein, we report the experimental thermodynamic hydricity of a new ruthenium CO_2 hydrogenation catalyst (^{acri}PNP)RuH(CO)(PPh$_3$) (**1**) supported by a rigid, acridane-based PNP pincer ligand. We provide the synthesis, structure, and spectroscopic characterization of reaction intermediates involved in formate generation including the anionic dihydride (**2**), formate (**3**), five-coordinate purple species (**4**), and H_2-bound species (**5**). Notably, the effective hydricity of complexes **1** and **2** in THF was determined by the H_2 heterolysis method, revealing values of >52 and 32 kcal/mol, respectively. The corresponding hydricity values of 45−48 kcal/mol for related Ru dihydride complexes supported by neutral PNP pincer ligands highlight the effect of anionic complex charge in promoting stronger hydride donors. CO_2 insertion into the Ru−H bond of the dihydride complex proceeds effectively under ambient conditions, suggesting that base-promoted H_2 heterolysis is the rate-limiting step. Using **1** as a precatalyst, turnover frequencies in the order of 300 h^{-1} were obtained for formate generation. Broadly, our results provide valuable benchmark thermochemical data for the design of improved CO_2 hydrogenation catalysts.

KEYWORDS: ruthenium, pincer ligands, metal-hydride complexes, CO_2 hydrogenation, hydricity

INTRODUCTION

Toward mitigating the effect of increasing atmospheric CO_2 concentration and developing a sustainable chemical industry, processes for CO_2 conversion into value-added products have received much attention.[1−3] In particular, extensive studies have been performed to develop efficient catalysts for the hydrogenation of CO_2 into C_1 chemicals such as formic acid and methanol as chemical feedstocks and liquid fuels.[4] Following an early report for the catalytic hydrogenation of CO_2 to formate using Raney nickel,[5] various homogeneous and heterogeneous transition metal catalysts have been developed.[6,7] Notably, some of the most efficient formate generating catalysts are based on Ru and Ir hydride complexes supported by pincer-type ligands that feature diphosphino amine or

pyridine moieties (Figure 1).[8,9] Highly effective systems based on first-row transition metals have also been described, encouraging further studies in the chemistry of metal hydrides for CO_2 reduction.[10−12]

In this regard, understanding how stereoelectronic effects influence hydride transfer reactivity is critical in the design of
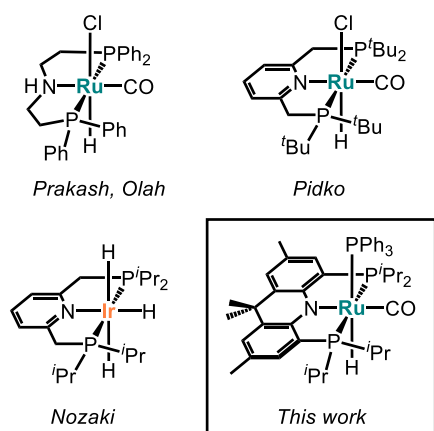
Figure 1. Selected examples of PNP pincer-supported metal hydride complexes for catalytic CO_2 hydrogenation.

CO_2 hydrogenation catalysts.[13,14] While certain processes may operate under kinetic control, thermodynamic parameters such as hydricity can provide important design criteria for new synthetic systems.[15] Hydricity $(\Delta G^{\circ}_{H^-})$ is defined as the free energy required to remove a hydride anion H^- from a species, according to the general reaction $M-H \rightarrow M^+ + H^-$.

The heterolytic cleavage of a $M-H$ bond to generate H^- is typically endergonic, and thus species with low hydricity values are considered strong hydride donors. This propensity to release H^- can be used to define reaction driving forces and predict reactivity. Similar thermodynamic considerations have

been applied for electrocatalytic CO_2 reduction and H_2 evolution/oxidation.[16,17] However, given the importance of Ru hydride complexes as hydrogenation catalysts, data regarding their hydricity remain rare. With the exception of two reports describing the thermodynamics of Ru PNP complexes in THF,[18,19] essentially all of the data is reported in either MeCN or H_2O for a series of ruthenium polypyridine complexes.[20] Importantly, since MeCN is rarely used in catalysis,[21] obtaining hydricity values in solvents such as THF for a wider range of catalytically relevant Ru hydride complexes is highly desirable.

Considering the prevalence of metal-pincer moieties in catalysis, careful consideration of ligand design is critical, and diverse PNP pincer ligands featuring dialkyl- or diarylphosphine moieties tethered to a nitrogen-containing backbone have been synthesized. Ru complexes with disilylamide, diarylamide, pyrrolide, acridine, pyridine, and diethylamine pincer backbones have been extensively studied.[22−28] In particular, metal-pincer systems that may display metal−ligand cooperativity via incorporation of weakly acidic N−H or C−H moieties have emerged as promising hydrogenation catalysts.[29] While initially thought to serve as proton donors, recent studies suggest that such functional moieties may stay intact in many catalytic applications and that fully deprotonated, anionic systems may show improved reactivity.[30] In this regard, we envisioned that such anionic Ru−H motifs can be more easily supported with an anionic acridane pincer backbone, while also improving the stability of the resulting catalyst.[31]
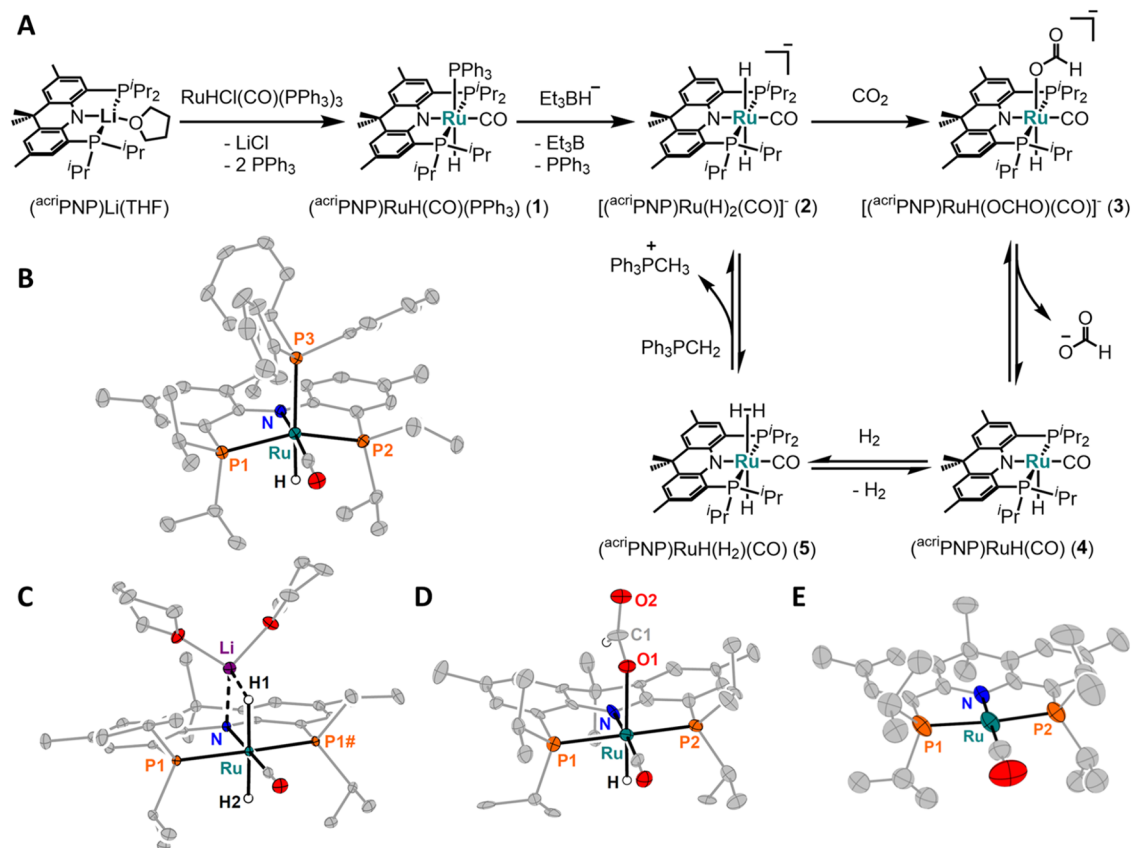

Figure 2. (A) Synthesis of the ^{acri}PNP-supported Ru complex **1** for base-promoted CO_2 hydrogenation to formate and synthetic route of intermediate species **2-5** involved in the catalytic cycle. Truncated displacement ellipsoid (50%) representations of (B) **1**, (C) **2**, (D) **3**, and (E) **4**.
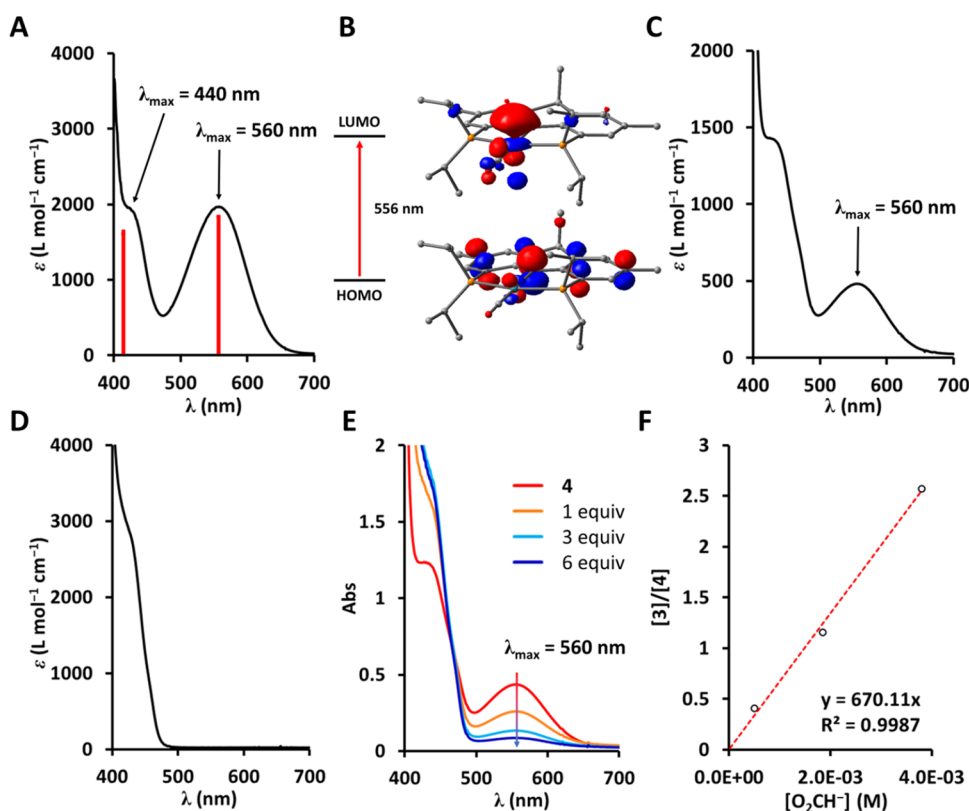
Figure 3. (A) UV−vis absorption spectrum of **4** in pentane. The red bars indicate the TD-DFT predicted electronic transitions. (B) Calculated frontier orbitals of **4** involved in the 556 nm transition rendered at 0.055 e/au^3. UV−vis spectrum of **4** in (C) THF, (D) MeCN, (E, F) upon addition of [^{n}Bu$_4$N][OCHO] in THF, and fit of the data to obtain the formate binding equilibrium constant.

Herein, we report a new ruthenium CO_2 hydrogenation catalyst supported by a rigid, acridane-based PNP pincer ligand.[32,33] We provide detailed structural and spectroscopic characterization of key reaction intermediates involved in formate generation. For an anionic Ru dihydride complex, the effective hydricity in THF was measured at 32 kcal/mol (calc. 30 kcal/mol). This value is significantly lower than that of 45−48 kcal/mol for related Ru dihydride complexes supported by neutral PNP ligands, highlighting the effect of anionic complex charge in promoting stronger hydride donors.[18] Consistent with this strong hydridic character, CO_2 insertion into the dihydride complex proceeds effectively under ambient conditions. Furthermore, the anionic charge of the complexes facilitates formate dissociation, suggesting that base-promoted H_2 heterolysis may be the rate-limiting step. Using **1** as a precatalyst, turnover frequencies in the order of 300 h^{-1} were obtained for formate generation. Broadly, our results provide valuable benchmark thermochemical data for the design of improved CO_2 hydrogenation catalysts that take into account the overall charge of the complex and the properties of the *trans* ligand for fine-tuning hydricity.

RESULTS AND DISCUSSION

Complex Synthesis

Building upon our previous effort in the chemistry of first-row transition metal pincer complexes for CO_2 activation,[11,32−41] related Ru complexes were targeted as catalysts for CO_2 conversion. While bis(phosphinoethyl)amine and 2,6-bis-(phosphinomethyl)pyridine PNP ligand frameworks have been studied extensively as neutral and potentially deproto-

nated, anionic ligands under basic reaction conditions, CO_2 hydrogenation catalysts supported by anionic acridane or diphenylamide PNP ligand frameworks remain rare aside from our previous work with a (PNP)CoH species.[11] Treatment of the Ru precursor RuHCl(CO)(PPh$_3$)$_3$ with (^{acri}PNP)Li(THF) results in the formation of complex **1** with the (^{acri}PNP)RuH-(CO)(PPh$_3$) formulation (Figure 2A). A similar complex was reported by Vogt and co-workers.[42] The ^{1}H NMR spectrum displays a doublet of triplets at −9.5 ppm corresponding to the hydride moiety, consistent with coupling to the ^{31}P atoms in Ph$_3$P ($^2J_{H-PPh_3}$ = 96 Hz) and ^{acri}PNP ($^2J_{H-PNP}$ = 20 Hz), see SI. Accordingly, the ^{31}P NMR spectrum displays a strongly coupled doublet at 27 ppm and a broad singlet at 77 ppm corresponding to the PPh$_3$ and ^{acri}PNP moieties, respectively. The single-crystal X-ray diffraction (SC-XRD) data indicate that a Ph$_3$P ligand coordinates at the axial site of the Ru(II) center *trans* to the hydride, while a carbonyl ligand occupies the equatorial position *trans* to the central amide of the ^{acri}PNP ligand (Figure 2B). A significant distortion away from octahedral geometry is observed in **1**, particularly in the ∠(P1−Ru−P2) = 147.00(4)° angle. The corresponding angle of 158.52(2)° in the analogous [(Ph$_2$PCH$_2$CH$_2$)N]RuH(CO)-(PMe$_3$) complex suggests that steric effects influence the structure of **1**.[43] Accordingly, a slightly elongated Ru−P3 distance of 2.477(1) Å is also observed in **1**, suggesting that catalytic CO_2 hydrogenation is likely initiated upon loss of Ph$_3$P. Subsequent binding and base-promoted heterolysis of H_2 would lead to an anionic dihydride species. To study the formation of such a species, complex **1** was treated with Li[Et$_3$BH], resulting in the formation of Li[(^{acri}PNP)Ru(CO)-(H)$_2$] (**2**). The ^{1}H NMR spectrum in THF-d_8 displays a

distinctive triplet at −7.0 ppm ($^2J_{H-PNP}$ = 20 Hz) corresponding to the hydride moieties. Accordingly, the ^{31}P NMR spectrum displays a triplet at 92.1 ppm, indicating that the two hydride moieties are chemically equivalent in solution. The SC-XRD data indicate the presence of two hydride moieties *trans* to each other at a six-coordinate ruthenium center (Figure 2C). In the solid state, the $[Li(THF)_2]^+$ moiety binds to the central amide of the ^{acri}PNP ligand featuring a Li−H−Ru bridging hydride interaction. This interaction is evident in the acute ∠(Li−N−Ru) angle of 79.96(14)° and the Li−H1 distance of 1.84(3) Å. Accordingly, elongated Ru−H1 and Ru−H2 distances of 1.72(4) and 1.64(4) Å are observed, respectively, compared to that of 1.58(3) Å in **1**. The elongated Ru−H distances in **2** can be attributed to the strong *trans* influence of the hydride ligand and the presence of Li−H Lewis acid interaction in the solid state. Computational studies suggest that ligands with strong *trans* influence weaken the metal−H bond and increase the nucleophilicity of the hydride.[44] Lewis acids such as Li$^+$ have also been shown to increase the rate of CO_2 insertion into metal hydrides, suggesting that rapid CO_2 insertion into the Ru−H1 bond of **2** may take place.[45] The structural parameters of **2** are similar to those of a Mn hydride complex featuring a Li−H−Mn interaction.[30] Related anionic ruthenium hydride complexes have been reported previously.[19,46,47] With the synthesis of the catalytically important *trans*-dihydride intermediate fully established, hydride transfer reactivity to CO_2 was further explored.

CO$_2$ Reactivity

Treatment of a THF solution of **2** with CO_2 at room temperature results in an immediate reaction accompanied by a color change from greenish yellow to purple. Concomitant formation of a white precipitate was observed, which was determined to be about one equivalent of lithium formate according to ^1H NMR data in D_2O. The observed reactivity is consistent with the initial formation of an anionic Ru formate species (**3**) (Figure 2A). Subsequent loss of formate results in the formation of the purple species as a five-coordinate Ru complex (**4**) or a solvento species (**4-THF**). The filled d_π orbitals of Ru parentage may contribute toward the loss of formate via d_π−p_π repulsive interactions.[48] The ^1H NMR spectrum in THF-d_8 displays a new hydride triplet at −21.2 ppm ($^2J_{H-P}$ = 20 Hz), see the SI. Accordingly, the ^{31}P NMR spectrum displays a doublet at 71.5 ppm ($^2J_{H-P}$ = 19 Hz). To obtain further insight into the structure of **4**, UV−vis absorption spectroscopic studies were performed in different solvents. Complex **4** reveals a purple color in pentane solution, showing a distinctive absorption band at 560 nm (1968 L mol^{-1} cm^{-1}) (Figure 3A). This absorption band completely disappears in CH_3CN solution, accompanied by a rapid color change to greenish yellow (Figure 3D). This result indicates that strongly coordinating solvents lead to the formation of a six-coordinate species similar to **1**. Interestingly, a THF solution of **4** reveals the presence of the absorption band at 560 nm (478 L mol^{-1} cm^{-1}) albeit in decreased intensity (Figure 3C). This implies that THF partially binds to the empty coordination site of **4** with an equilibrium constant of K_{eq} = 3.1, with the assumption that the extinction coefficient of the five-coordinate species **4** is the same in both pentane and THF. The intensity of the calculated absorption band at 556 nm of **4** matches well with the experimental spectrum in pentane (Figure 3A), *vide infra*. To assign the electronic

transition at 560 nm, time-dependent density functional theory calculations were conducted on **4**. Results show that this transition is due to the ligand-to-metal charge transfer (LMCT) transition between the HOMO and the LUMO of **4** (Figure 3B). The HOMO is primarily of ligand character, containing the π-orbitals of the acridane backbone. As expected, the LUMO is primarily of Ru d_{z^2} orbital character, consistent with a Ru(II) low-spin d^6 electronic configuration. The absence of this absorption band in the six-coordinate complexes can be explained in terms of the higher energy of the Ru d_{z^2} orbital as it assumes a more pronounced σ-antibonding character, suggesting that the transition at 560 nm undergoes a hypsochromic shift upon ligand binding. The SC-XRD data further support the $(^{acri}PNP)RuH(CO)$ formulation of **4** (Figure 2E). The location of the hydride moiety could not be located in the crystal structure due to disorder, consistent with a five-coordinate species positioned in two orientations with respect to the Ru−H vector (i.e., the hydride located above or below the plane defined by the ^{acri}PNP ligand). Accordingly, the CO ligand is disordered in two distinctive positions, indicating a small deviation from a perfectly square pyramidal geometry around the Ru center (see the SI). Further support for the structure of **4** was established via electrospray ionization mass spectrometry (ESI-MS) data (see the SI). By adding increasing amounts of soluble $[^nBu_4N][OCHO]$ to a THF solution of **4**, quenching of the absorption band at 560 nm (Figure 3E) and formation of an anionic, octahedral Ru formate species **3** was observed (Figure 2A). ESI-MS data also supports the formation of **3** (see the SI). Yellow single crystals of **3** were obtained from THF solution in the presence of 20 equiv of $[^nBu_4N][OCHO]$ (Figure 2D). The SC-XRD data indicate a formate ligand coordinated to the Ru(II) center *trans* to hydride, as expected from CO_2 insertion into the dihydride species **2**. Interestingly, the Ru−O1 distance of 2.275(8) Å in **3** is slightly longer than previously reported examples, consistent with the observed labile character of the formate.[26,48,49] The equilibrium constant of formate binding to **4** was obtained (Figure 3F), leading to a formate dissociation free energy of 4 kcal/mol from **3**. In comparison, formate dissociation free energies of 13−19 kcal/mol were calculated for related, neutral (PNP)Ru complexes featuring a similar coordination environment with a hydride *trans* to the formate moiety.[49] Thus, the lower formate dissociation energy of **3** is attributed to the anionic charge of the complex. With the hydride transfer reactivity to CO_2 fully established, the thermodynamic hydricity of **2** was further studied.

Thermodynamic Hydricity

To obtain further insight into the thermodynamics of hydride transfer reactivity, the hydricity of complex **2** was determined in THF (Figure 4). Having measured the equilibrium constant for the binding of THF to the five-coordinate species **4** (K_{eq2}), measuring the energy of the heterolytic cleavage of H_2 (K_{eq1}) yields the effective hydricity of **2**.[13] This can be achieved via spectrophotometric titration of **2** with an appropriate acid under 1 atm of H_2. To help narrow down the pK_a of the acid that would result in a measurable equilibrium constant, DFT calculations were also performed. On the basis of the calculated energies of complexes **2** and **4** corrected for dissolution in THF, a hydricity of ΔG_{H^-} = 30.6 kcal/mol was obtained. Considering the free energy of THF binding to **4** (ΔG_2 = −0.7 kcal/mol), a calculated effective hydricity of $\Delta G_{H^-}(THF)$ ≈ 30 kcal/mol was obtained. Using the
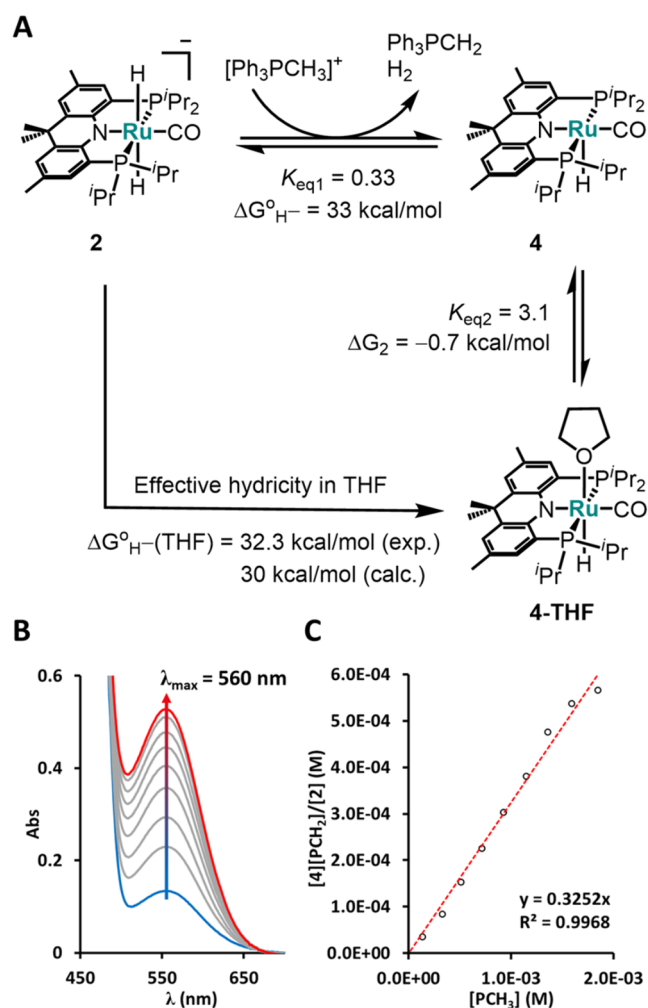
Figure 4. (A) Thermodynamic scheme for the effective hydricity of complex **2** in THF. (B) UV−vis spectrophotometric titration of **2** in THF with incremental addition of the phosphonium $[Ph_3P-CH_3][BPh_4]$ as acid. (C) Fit of the data to obtain the equilibrium constant.

Table 1. Comparison of Hydricity Values Reported in THF[a]

complex	hydricity (kcal/mol)	refs
$[(^iPr_2PEt-)_2NH)Fe(H)_2(CO)]$	59.3−62.4[b]	19,56
$(SiP_3)Fe(H_2)H$	54.4	51
$(PNP)RuH(CO)(PPh_3)$ (**1**)	>**52**	d
$[(Cy_2PEt-)_2NH)Ru(H)_2(CO)]$	~**48**	19
$(PNP)M(H)_2(CO)$ (M = Mn, Fe, Co, Ru)	43.6−44.6	18
$[(P_3N_4)MCo(H_2)]^-$ (M = Al, Ga)	35.4, 40.5[c]	52
$[(P_3N_4)MNiH]^-$ (M = B, Al, Ga, In)	21.4, 31.8, 34.7, 39.2[c]	57
$[(PCP)ReH(CO)_2]^-$	37.6	21
$[(PNP)M(H)_2(CO)]^-$ (M = Fe, Ru)	27.7, **30.0**[c]	19
$[(PNP)Ru(H)_2(CO)]^-$ (**2**)	**32**	d

[a]Ru complexes highlighted in bold. [b]Two separate values reported. [c]Respectively, in the order shown. [d]This work.

anionic $[(PNP)Ru(H)_2(CO)]^-$ complex was measured at 30 kcal/mol, showing that large changes in hydricity can be observed based on complex charge.[19] Furthermore, the nature of the rigid pincer backbone of an $(^{acri}PNP)Ru$ scaffold allows two hydride ligands to be firmly located *trans* to each other, effectively providing a strong *trans influence* on each other and increasing the hydricity of **2**.

To provide further comparison, the hydricity of **1** was measured using the conjugate acids of TBD (pK_a = 21.0), DBU (pK_a = 16.9), pyrrolidine (pK_a = 13.5), and Et_3N (pK_a = 12.5). In all four cases, no reactivity was observed, indicating that the hydricity of **1** is greater than 52 kcal/mol (see the SI). Compared to that of complex **2**, such a dramatic shift in hydricity of more than 20 kcal/mol is noteworthy. For an anionic Re−H complex with a *trans* carbonyl ligand as a weaker σ donor than hydride, a hydricity of 38 kcal/mol was obtained, suggesting that further fine-tuning of hydricity can be achieved with diverse *trans* donors.[21] While analogous examples of structurally similar complexes that differ only by the overall charge are difficult to find, hydricity values for a few redox series have been reported: $[Co(dppe)_2H]^{+/0}$, $[CpW-(CO)_2(IMes)H]^{+/0}$, $[Ru(terpy)(bpy)H]^{+/2+}$.[20,53,54] In all three cases, the more reduced complexes are more hydridic, by 10.6, 10.8, and 17.3 kcal/mol, respectively. In a series of highly analogous Rh hydride complexes, steric and electronic effects influence hydricity by as much as 22 kcal/mol without changes in oxidation state; when solvent binding is involved, smaller phosphine ligands lead to more hydridic species, but otherwise, more electron rich ligands support stronger hydride donors.[55] Combined, our results underscore the importance of careful catalyst design that incorporates into consideration the overall charge of the complex for controlling the thermodynamic driving force of hydride insertion into unsaturated moieties.

H_2 Binding

For better understanding of the formation of the dihydride complex **2**, the reactivity of the five-coordinate purple species **4** with H_2 was explored. Upon cooling a toluene solution of **4** under an atmosphere of H_2, a decrease in the intensity of the absorption band at 560 nm was observed (see the SI). This is consistent with the formation of a six-coordinate species through H_2 binding, with an estimated H_2-binding equilibrium constant of K_{eq} = 0.38 at room temperature. This process was additionally monitored by variable temperature ^1H NMR spectroscopy in toluene-d_8 (see the SI). As shown in Figure 5, the triplet at −25 ppm corresponding to the hydride moiety of **4** becomes broad and shifts downfield upon H_2 addition and cooling. Upon further cooling to −85 °C, a triplet at −9.6 ppm

phosphonium $[Ph_3P-CH_3][BPh_4]$ with a pK_a = 26.6 in THF,[50] an equilibrium was established between **2** and **4**, and a value of K_{eq1} = 0.33 was obtained after mass balance considerations (Figure 4c). In comparison, an equilibrium constant of K_{eq1} = 0.2 was obtained using ^{31}P NMR, see SI. Using the value of ΔG_{H2} = 68.7 kcal/mol for the free energy of H_2 heterolysis in THF, this corresponds to an experimental hydricity of ΔG_{H^-} = 33 kcal/mol and an effective hydricity of $\Delta G_{H^-}(THF) \approx 32$ kcal/mol for **2**. Because THF binding to **4** is nearly thermoneutral, the hydricity values with or without THF binding are within the experimental error of ~1 kcal/mol. While hydricity values have been determined for a wide variety of metal hydride complexes in MeCN, hydricity data in a catalytically more relevant solvent such as THF have only recently been reported.[18,19,21,51,52] In the case of Ru hydride species, hydricity values of 45−48 kcal/mol have been reported for $(PNP)Ru(H)_2(CO)$ complexes supported by neutral PNP pincer ligands featuring pyridine or secondary amine donors (Table 1).[18] Considering the similar coordination sphere between these complexes and **2**, the noticeably more hydridic character of **2** by 13−15 kcal/mol can be attributed to the anionic charge of **2**. In fact, the hydricity of a deprotonated,
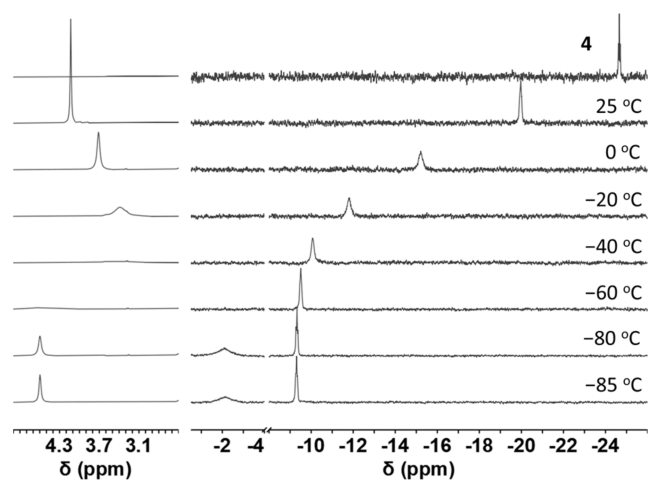
Figure 5. Truncated, variable temperature ^1H NMR spectra of complex **4** in the presence of H_2.

can be partially resolved, in addition to a broad, uncoupled signal at −2 ppm. Tentatively, we assign the signal at −9.6 ppm to a hydride moiety and the signal at −2 ppm to a dihydrogen moiety with a $(^{acri}PNP)RuH(H_2)(CO)$ formulation (**5**) (Figure 2A). Solution ^1H NMR spectra of η^2-H_2 ligands typically give such broad uncoupled signals.[58,59] The ^{31}P NMR spectra collected under H_2 show similar temperature dependence, with the initial doublet at 72 ppm of **4** shifting to a broad singlet at 82 ppm corresponding to **5**. Similar Ru dihydrogen complexes have been reported with PNP and POP pincer ligands.[60−62] Finally, treatment of **4** with $Ph_3P = CH_2$ as a base in the presence of H_2 generates an equilibrium mixture of **4** and **2**, see the SI. These results suggest the formation of a hydride-dihydrogen complex consistent with **5**, closing the synthetic cycle for the hydrogenation of CO_2 to formate at an ^{acri}PNP-supported Ru center.

Catalytic Studies

Initially, the catalytic activity of **1** toward CO_2 hydrogenation to formate was explored. Reaction conditions with high pressure CO_2/H_2 generally result in improved yields (see the SI).[63] Keeping the pressure constant at 40 bar of 2:2 CO_2/H_2, the effect of different bases was studied (Table 2, entries 1−5). At 150 °C, the soluble organic base DBU (1,8-diazabicyclo[5.4.0]undec-7-ene) gave very poor yields of formate. This is in stark contrast to the impressive turnover frequency of 1.1×10^6 h^{-1} reported for a neutral PNP-Ru complex using DBU as a base.[9] Considering the $\Delta G_{H^-} \approx 32$ kcal/mol for **2**, this indicates that the base-promoted H_2 heterolysis step is endergonic, with a $\Delta G[kcal/mol] = 36.7 − 1.364(pK_a)$ at room temperature. With DBU, this translates to an uphill process by ∼14 kcal/mol, close to the driving force of ∼13 kcal/mol for hydride insertion into CO_2 to generate formate. Thus, future catalyst design should focus on obtaining metal hydricity values near the formate hydricity value of ∼45 kcal/mol to operate at near thermoneutral conditions. Using inorganic bases such as KOH and K_3PO_4 at 150 °C, decent to good yields of formate were obtained. At increased amounts of K_3PO_4, turnover numbers of up to ∼10^3 were obtained after 24 h. Encouraged by these results, a series of alkali metal bases were tested (Table 2, entries 6−11) under reaction conditions that would entropically favor the H_2 heterolysis step (lower temperature). Using water as a cosolvent at 60 bar of 3:3 CO_2:H_2 and 75 °C, Na_3PO_4 was identified as a particularly

Table 2. Catalytic CO_2 Hydrogenation to Formate[a]

entry	base	formate (mmol)[b]	TON	TOF (h^{-1})
1−5: 10 mL THF, 40 bar 2:2 CO_2:H_2, 150 °C, 24 h				
1	DBU (10 mmol)	0.13	6.6	0.3
2	KOH (10 mmol)	6.23	312	13
3	K_3PO_4 (5 mmol)	2.16	108	5
4	K_3PO_4 (10 mmol)	8.23	412	17
5	K_3PO_4 (20 mmol)	18.71	936	39
6−11: 10 mL/5 mL THF/H_2O, 60 bar 3:3 CO_2:H_2, 75 °C, 5 h				
6	LiOH (25 mmol)	3.56	178	36
7	NaOH (25 mmol)	2.41	121	24
8	KOH (25 mmol)	5.43	271	54
9	Li_3PO_4 (25 mmol)	0.53	27	5
10	Na_3PO_4 (25 mmol)	8.19	410	82
11	K_3PO_4 (25 mmol)	5.49	275	55
12: 10 mL/5 mL THF/H_2O, 80 bar 3:5 CO_2:H_2, 75 °C, 5 h				
12	Na_3PO_4 (25 mmol)	11.39	569	114
13−15: 10 mL/5 mL THF/H_2O, 100 bar 3:7 CO_2:H_2, 75 °C, 5 h				
13	Na_3PO_4 (25 mmol)	28.25	1412	282
14[c]	Na_3PO_4 (25 mmol)	0.07	3.5	0.7
15[d]	Na_3PO_4 (25 mmol)	17.07	853	171

[a]Using 20 μmol of **1** as precatalyst. [b]Obtained from integration of formate ^1H NMR signal using 1,3,5-trimethoxybenzene as internal standard. [c]Using 20 μmol of **4** as precatalyst. [d]Using 20 μmol of $[(Ph_2PEt−)_2NH]RuHCl(CO)$ (Ru-MACHO) as precatalyst.

effective base for formate generation (Table 2, entry 10). Under otherwise identical conditions, increasing the H_2 pressure led to a significant increase in formate yield, reaching turnover frequencies in the order of ∼300 h^{-1} over 5 h (Table 2, entry 13). This catalyst behavior suggests that the H_2 heterolysis step leading to the formation of the dihydride species may be the rate-limiting step, with CO_2 insertion into Ru−H and formate loss being very facile according to our stoichiometric reactivity studies *vide supra*. Such an inverse temperature dependence on turnover frequency has been observed in a related system.[21] Using **4** as the precatalyst led to poor formate yield (Table 2, entry 14), indicating that the presence of Ph_3P is necessary to prevent catalyst decomposition. To further compare the activity of **1**, the commercially available catalyst $[(Ph_2PEt−)_2NH]RuHCl(CO)$ (Ru-MACHO) was used for formate generation (Table 2, entry 15). Results show a slightly decreased activity compared to that of **1**, with a TOF of ∼170 h^{-1}. For the MACHO system, TOF values in the range of 200−2000 h^{-1} have been reported, depending on experimental conditions.[64] Compared to **1**, the lower activity of Ru-MACHO may be related to the turnover-limiting formate dissociation step,[49] suggesting that formate dissociation is facilitated by a negative complex charge. Interestingly, Vogt and co-workers reported that Ru-PNP complexes bearing secondary amines were ineffective for the transfer hydrogenation of alcohols to amines, while ligands with tertiary amines gave active catalysts.[42] In this regard, the observed catalytic activity toward CO_2 hydrogenation offers a distinct possibility that **1** is a competent catalyst for transfer hydrogenation, and this line of questioning will be uncovered in future studies.

With the catalytic activity of **1** toward CO_2 hydrogenation to formate established, strategies to convert formate to further reduced products such as formaldehyde and methanol through amine-promoted pathways were explored.[4] Under catalytic conditions, ammonium formates generated via CO_2 hydro-

genation condense to give formamides as key intermediates for reduced C_1 chemicals. Keeping the pressure constant at 80 bar of 1:3 CO_2/H_2, the effect of different amine bases was studied (Table 3). At 150 °C, poor turnover was observed with tertiary

Table 3. Catalytic CO_2 Hydrogenation to Formamide[a]

entry	base[b]	formamide (mmol)[c]	TON	TOF (h⁻¹)
	20 mL THF, 80 bar of 2:6 CO_2:H_2, 150 °C, 24 h[d]			
1	Et₃N	0.12	0.12	5×10^{-3}
2	EN	1.2	120	5
3	N,N′-DMEDA	3.63	363	15
4	N,N-DMEDA	2.08	208	9
5	TMEDA	0.067	0.67	3×10^{-2}
6	DETA	9.22	922	38
7	PEHA	9.39	939	39
8	PEHA	19.67	1967	41

[a]Using 10 μmol of **1** as precatalyst. [b]10 mmol base used. Abbreviations: EN: ethylenediamine, N,N′-DMEDA: N,N′-dimethylethylenediamine, N,N-DMEDA: N,N-dimethylethylenediamine, TMEDA: tetramethylethylenediamine, DETA: diethylenetriamine, PEHA: pentaethylenetriamine. [c]Obtained from integration of formamide ¹H NMR signal using 1,3,5-trimethoxybenzene as internal standard. [d]48 h for entry 9.

amines (Table 3, entries 1 and 5), as only primary or secondary amines can generate formamides via condensation with formate. With ethylene diamine and dimethylated derivatives as base (Table 3, entries 2−4), improved formamide turnover was observed with the N,N′ disubstituted diamine, indicating that formation of formamides from secondary amines is more favorable. With longer polyethylene amines as base (Table 3, entries 6−8), turnover numbers in the order of 10^3 cycles were obtained, with no significant loss of activity over 48 h. While more reduced compounds such as methanol have not been detected thus far, further catalyst optimization studies are underway to discover conditions that would allow the conversion of secondary formamides to aminal species, and preliminary reactivity studies indicate that the dihydride complex **2** reacts with dimethylformamide at ambient conditions and these results will be reported in due course.

CONCLUSIONS

A new ruthenium CO_2 hydrogenation catalyst supported by a rigid PNP pincer was synthesized and characterized. The intermediates of CO_2 hydrogenation to formate were thoroughly studied via structural, spectroscopic, and computational methods revealing an anionic dihydride **2** with an experimental thermodynamic hydricity of 32 kcal/mol in THF. The strong hydridic nature of this species can be attributed to the charge and the *trans* influence of the dihydride moiety resulting from a structurally rigidified [acri]PNP pincer ligand. Notably, the hydricity of the neutral hydride species **1** featuring a *trans* PPh₃ ligand is estimated to be greater than 52 kcal/mol, representing a shift of more than 20 kcal/mol. Our studies provide important thermodynamic benchmarking results for future catalyst designs, in which the overall charge of the complex and the properties of the *trans* ligand are taken into consideration for fine-tuning hydricity. Specifically, metal hydricity values near that of the target product such as formate should be targeted to avoid large changes in the potential energy surface and minimize barriers in the catalytic process.

MATERIALS AND METHODS

General Considerations

All manipulations were carried out using standard Schlenk or glovebox techniques under N₂ or Ar atmosphere. Unless otherwise noted, solvents were deoxygenated and dried by thoroughly sparging with Ar followed by passage through an activated alumina column. Nonhalogenated solvents were tested with a standard purple solution of sodium benzophenone ketyl in tetrahydrofuran in order to confirm effective oxygen and moisture removal. All reagents were purchased from commercial vendors and used without further purification unless otherwise stated. Elemental analyses of complex **1** and **2** were carried out at Sogang Center for Research Facilities on Thermo Scientific FLASH 2000 series instrument.

X-ray Crystallography

The diffraction data of complexes **1−4** were collected on a Bruker D8 QUEST instrument. Suitable crystals were coated with Paratone-*N* oil and mounted on a Dual-Thickness MicroLoops LD purchased from MiTeGen. The data were collected with graphite-monochromated Mo Kα radiation (λ = 0.71073 Å) under a stream of N₂ at 100 K. The structures were solved by direct methods, and all non-hydrogen atoms were subjected to anisotropic refinement by full-matrix least-squares on F^2 by using the SHELXTL/PC package.[65,66] Hydrogen atoms were placed at their geometrically calculated positions and refined, riding on the corresponding carbon atoms with isotropic thermal parameters. Full crystallographic details can be obtained free of charge from the Cambridge Crystallographic Data Center via CCDC deposition numbers 2380485−2380488.

Characterization

An Agilent 400-MR spectrometer was used to measure room temperature ¹H and ³¹P NMR spectra at the chemistry department of Seoul National University; a Bruker AVANCE III HD-400 spectrometer was used to measure variable temperature ¹H and ³¹P NMR spectra at the chemistry department of the Korea Advanced Institute of Science and Technology. Deuterated solvents were purchased from Deutero, degassed, and dried over activated 4 Å molecular sieves prior to use. The chemical shifts for ¹H NMR spectra are quoted in parts per million (ppm) and are referenced to residual solvent peaks. The chemical shifts for ³¹P NMR spectra are quoted in parts per million (ppm) and are referenced to external phosphoric acid in D₂O at 0.00 ppm. Coupling constants J are reported in Hertz (Hz). Low-temperature UV−vis spectra were measured using an Agilent Cary 8454 UV−vis spectrophotometer equipped with a UNISOKU Scientific Instruments cryostat. Infrared spectra were recorded in KBr pellet using Bruker VECTOR 33. Frequencies are given in reciprocal centimeters (cm⁻¹) and only selected absorbances are reported. Electrospray ionization mass (ESI-MS) spectra were obtained using a Thermo Scientific LTQ XL linear ion trap mass spectrometer. All sample solutions were directly infused into the mass analyzer using a syringe pump. The temperature of the MS capillary inlet was set to 250 °C and the tube lens voltage was set at 4.5 kV.

Computational Methods

The initial geometries for the computational models were obtained from the corresponding X-ray crystal structures. Density functional theory (DFT) geometry optimization calculations were performed with the B3LYP functional[67] and Def2SVP basis set[68] using the Gaussian 16 package.[69] The optimized geometries were verified using frequency calculations to confirm the absence of any imaginary frequencies. Using the optimized geometries, thermochemical analysis was performed using the calculated Gibbs free energies obtained with the M062X functional[70] and Def2TZVP basis set.[68] The solvent effects were included using the CPCM model for THF.[71,72]

Synthesis of ([acri]PNP)RuH(CO)(PPh₃) (1)

An oven-dried Schlenk tube (100 mL) was charged with RuHCl-(CO)(PPh₃)₃ (1.823 mmol, 1.743 g), ([acri]PNP)Li(THF) (1.896 mmol, 1.038 g), and toluene. The sealed Schlenk tube was then heated to 110 °C and stirred for 3 h. Upon cooling, all volatiles were

removed under reduced pressure. Benzene (20 mL) was added to dissolve the residue, filtered through Celite, and dried under reduced pressure. The residue was redissolved in pentane (30 mL) and stored at −35 °C to induce precipitation. The resulting product (^{acri}PNP)-RuH(CO)(PPh$_3$) (**1**) (1.588 mmol, 1.367g, 75%) was isolated as a yellow powder after washing three times with 10 mL of cold pentane and drying under reduced pressure. ^{1}H NMR (400 MHz, Toluene-d_8): δ 7.46−7.41 (m, 6H), 7.11−7.08 (m, 4H), 6.92−6.90 (m, 9H), 2.45−2.30 (m, 8H), 1.85−1.77 (m, 2H), 1.71 (m, 3H), 1.35−1.26 (m, 12H), 1.20−1.14 (q, 6H), 0.93 (s, 3H), 0.89−0.83 (q, 6H), −9.45 − −9.69 (dt, $^2J_{H-PPh3}$ = 96 Hz, $^2J_{H-PNP}$ = 20 Hz, 1H), ^{31}P NMR (162 MHz, Toluene-d_8): δ 76.86 (s), 27.07−26.46 (d, $^2J_{PPh3-H}$ = 99 Hz). Anal. Calcd for C$_{48}$H$_{60}$NOP$_3$Ru: C, 66.96; H, 7.02; N, 1.63. Found: C, 66.89; H, 7.04; N, 1.65. UV−vis [THF, nm (L mol^{-1} cm^{-1})]: 350 (420), 400 (100), 440 (44). X-ray quality single crystals were grown by layer diffusion of pentane into a saturated THF solution of **1**.

Synthesis of Li[(^{acri}PNP)Ru(CO)(H)$_2$] (2)

At room temperature, a solution of complex **1** (0.483 mmol, 0.42 g) in THF was treated with 0.58 mL of 1 M superhydride solution in THF (0.58 mmol, 0.061 g) and stirred for 12 h. Subsequently, all volatiles were removed under reduced pressure. The resulting product Li[(^{acri}PNP)Ru(CO)(H)$_2$] (**2**) (0.309 mmol, 0.188 g, 64%) was isolated as a greenish white powder after washing with 10 mL of benzene followed by 10 mL of pentane three times and drying under reduced pressure. ^{1}H NMR (400 MHz, THF-d_8): δ 6.89 (s, 2H), 6.81 (m, 2H), 2.25−2.18 (m, 10H), 1.36−1.31 (m, 18H), 1.12−1.06 (q, 12H), −6.94 − −7.94 (t, $^2J_{H-PNP}$ = 20 Hz, 2H). ^{31}P NMR (162 MHz, THF-d_8): δ 92.14 (s). Anal. Calcd for C$_{30}$H$_{46}$LiNOP$_2$Ru: C, 59.40; H, 7.64; N, 2.31. Found: C, 59.31; H, 7.84; N, 2.23. UV−vis [THF, nm (L mol^{-1} cm^{-1})]: 350 (744), 400 (183), 440 (85). X-ray quality single crystals were grown by layer diffusion of pentane into a saturated THF solution of **2**.

Formation of [^{n}Bu$_4$N][(^{acri}PNP)RuH(CO)(OCHO)] (3)

Into the solution of **4** (0.835 mmol, 0.050 g) in 3 mL THF, [^{n}Bu$_4$N][OCHO] (1.67 mmol, 0.480 g) was added and stirred for 10 min at room temperature. The resulting product was obtained as yellow crystal after crystallization grown by layer diffusion of pentane into a prepared mixture solution.

Synthesis of (^{acri}PNP)RuH(CO) (4)

A solution of complex **2** (0.181 mmol, 0.110 g) in 10 mL of THF was charged into an oven-dried 100 mL Schlenk tube. After three times of freeze−pump−thaw, CO$_2$ gas was injected into the Schlenk tube. Subsequently, reaction mixture was dried under reduced pressure and redissolved in 10 mL of pentane. The resulting product (^{acri}PNP)-RuH(CO) (0.176. mmol, 0.105 g, 97.2%) was isolated as purple solid after Celite filter with 50 mL of pentane and drying under reduced pressure. ^{1}H NMR (400 MHz, THF-d_8): δ 7.05 (s, 2H), 6.90 (m, 2H), 2.60−2.50 (m, 2H), 2.60−2.49 (m, 2H), 2.37−2.28 (m, 2H), 2.23 (s, 6H), 1.70 (s, 6H), 1.46−1.41 (m, 6H), 1.29−1.23 (m, 6H), 1.23 (m, 6H), 1.15 (m, 3H), 1.13−1.07 (m, 6H), 0.86−0.80 (m, 6H), −21.09 − −21.20 (t, 1H). ^{31}P NMR (400 MHz, THF-d_8): δ 71.63 (d, $^2J_{PNP-H}$ = 19 Hz). Anal. Anal. Calcd for C$_{30}$H$_{48}$LiNOP$_2$Ru: C, 60.18; H, 7.58; N, 2.34. Found: C, 60.24; H, 7.60; N, 2.26. UV−vis [Pentane, nm (L mol^{-1} cm^{-1})]: 556 (2028). [THF, nm (L mol^{-1} cm^{-1})]: 556 (460) X-ray quality single crystals were grown by H-grease assisted slow evaporation of saturated pentane solution of **4**.

Synthesis of the Phosphonium [Ph$_3$PCH$_3$][BPh$_4$]

At room temperature, a solution of [Ph$_3$PCH$_3$][I] (5.0 mmol, 2.02 g) in THF was treated with NaBPh$_4$ (5.0 mmol, 1.71 g) and stirred for 12 h. Subsequently, all volatiles were removed under reduced pressure. The residue was dissolved in CH$_2$Cl$_2$, filtered through Celite and dried under reduced pressure. The resulting product [Ph$_3$PCH$_3$][BPh$_4$] (4.9 mmol, 2.92 g, 98%) was obtained as a white powder. ^{1}H NMR (400 MHz, CD$_2$Cl$_2$): δ 7.84−7.80 (t, 3H), 7.66−7.61 (td, 6H), 7.41−7.34 (m, 14H), 7.00−6.96 (t, 8H), 6.85−6.81 (t,

4H), 7.00−6.96 (t, 8H), 1.99 (t, 3H). ^{31}P NMR (162 MHz, CD$_2$Cl$_2$): δ 21.32 (s).

Catalytic Hydrogenation of CO$_2$

The hydrogenation reactions were performed in a batch reactor. The specified amount of complex **1** and base were dissolved in THF and then added to the batch reactor. Before each experiment, a leak test was conducted on the batch reactor. To remove residual O$_2$, the reactor was pressurized with N$_2$ and purged three times. Subsequently, CO$_2$ was injected into the batch reactor to the specified pressure, followed by H$_2$ injection to the specified pressure. The reaction was carried out under heating (150 °C) and stirring (100 rpm). After the reaction for a given amount of time, the reactor was cooled to room temperature. The reaction mixture was collected from the reactor, and then pure H$_2$O (5−10 mL) was added to the mixture, which was stirred to form a homogeneous solution. The amount of product in solution was confirmed using an NMR instrument (400 MHz, Bruker Avance III HD 400). In more detail, 1,3,5-trimethoxybenzene (0.5 mmol) was dissolved in the homogeneous solution as an internal standard. This solution was analyzed by ^{1}H NMR with a few drops of D$_2$O.

■ ASSOCIATED CONTENT

Ⓢ Supporting Information

The Supporting Information is available free of charge at https://pubs.acs.org/doi/10.1021/jacsau.4c01078.

> Experimental details, spectroscopic data, X-ray crystallographic data, and DFT-calculated data for **1**−**5** (PDF)

Accession Codes

CCDC 2380485−2380488 contain the supporting crystallographic data for this paper. These data can be obtained free of charge via www.ccdc.cam.ac.uk/data_request/cif, or by emailing data_request@ccdc.cam.ac.uk, or by contacting The Cambridge Crystallographic Data Centre, 12 Union Road, Cambridge CB2 1EZ, U.K.; fax: + 44 1223 336033.

■ AUTHOR INFORMATION

Corresponding Authors

Heui Beom Lee − *Department of Chemistry, Seoul National University, Seoul 08826, Republic of Korea*; Email: heuibeomlee@snu.ac.kr

Yunho Lee − *Department of Chemistry, Seoul National University, Seoul 08826, Republic of Korea*; ⓘ orcid.org/0000-0002-9113-9491; Email: yunhochem@snu.ac.kr

Authors

Juwon Paik − *Department of Chemistry, Seoul National University, Seoul 08826, Republic of Korea*

Jong Hyeak Choe − *Clean Energy Research Center, Korea Institute of Science and Technology, Seoul 02792, Republic of Korea*

Sudakar Padmanaban − *Department of Chemistry, Seoul National University, Seoul 08826, Republic of Korea*; ⓘ orcid.org/0000-0001-8625-8480

Misook Seo − *Department of Chemistry, Seoul National University, Seoul 08826, Republic of Korea*

Chun-Jae Yoo − *Clean Energy Research Center, Korea Institute of Science and Technology, Seoul 02792, Republic of Korea; Division of Energy and Environment Technology, KIST School, University of Science and Technology, Seoul 02792, Republic of Korea; KIST-SKKU Carbon-Neutral Research Center, Sungkyunkwan University, Suwon 16419, Republic of Korea*; ⓘ orcid.org/0000-0002-1392-5817

REFERENCES

(1) Aresta, M.; Dibenedetto, A.; Angelini, A. Catalysis for the Valorization of Exhaust Carbon: from CO_2 to Chemicals, Materials, and Fuels. Technological Use of CO_2. *Chem. Rev.* **2014**, *114* (3), 1709−1742.

(2) Peters, M.; Köhler, B.; Kuckshinrichs, W.; Leitner, W.; Markewitz, P.; Müller, T. E. Chemical Technologies for Exploiting and Recycling Carbon Dioxide into the Value Chain. *ChemSusChem* **2011**, *4* (9), 1216−1240.

(3) Song, Q.-W.; Ma, R.; Liu, P.; Zhang, K.; He, L.-N. Recent progress in CO_2 conversion into organic chemicals by molecular catalysis. *Green Chem.* **2023**, *25* (17), 6538−6560.

(4) Sen, R.; Goeppert, A.; Prakash, G. K. S. Homogeneous Hydrogenation of CO_2 and CO to Methanol: The Renaissance of Low-Temperature Catalysis in the Context of the Methanol Economy. *Angew. Chem., Int. Ed.* **2022**, *61* (42), No. e202207278.

(5) Farlow, M. W.; Adkins, H. The Hydrogenation of Carbon Dioxide and a Correction of the Reported Synthesis of Urethans. *J. Am. Chem. Soc.* **1935**, *57* (11), 2222−2223.

(6) Kushwaha, S.; Parthiban, J.; Singh, S. K. Recent Developments in Reversible CO_2 Hydrogenation and Formic Acid Dehydrogenation over Molecular Catalysts. *ACS Omega* **2023**, *8* (42), 38773−38793.

(7) Álvarez, A.; Bansode, A.; Urakawa, A.; Bavykina, A. V.; Wezendonk, T. A.; Makkee, M.; Gascon, J.; Kapteijn, F. Challenges in the Greener Production of Formates/Formic Acid, Methanol, and DME by Heterogeneously Catalyzed CO_2 Hydrogenation Processes. *Chem. Rev.* **2017**, *117* (14), 9804−9838.

(8) Tanaka, R.; Yamashita, M.; Nozaki, K. Catalytic Hydrogenation of Carbon Dioxide Using Ir(III)−Pincer Complexes. *J. Am. Chem. Soc.* **2009**, *131* (40), 14168−14169.

(9) Filonenko, G. A.; van Putten, R.; Schulpen, E. N.; Hensen, E. J. M.; Pidko, E. A. Highly Efficient Reversible Hydrogenation of Carbon Dioxide to Formates Using a Ruthenium PNP-Pincer Catalyst. *ChemCatChem* **2014**, *6* (6), 1526−1530.

(10) Wei, D.; Sang, R.; Sponholz, P.; Junge, H.; Beller, M. Reversible hydrogenation of carbon dioxide to formic acid using a Mn-pincer complex in the presence of lysine. *Nat. Energy* **2022**, *7* (5), 438−447.

(11) Choi, J.; Lee, Y. Catalytic hydrogenation of CO_2 at a structurally rigidified cobalt center. *Inorg. Chem. Front.* **2020**, *7* (9), 1845−1850.

(12) Langer, R.; Diskin-Posner, Y.; Leitus, G.; Shimon, L. J. W.; Ben-David, Y.; Milstein, D. Low-Pressure Hydrogenation of Carbon Dioxide Catalyzed by an Iron Pincer Complex Exhibiting Noble Metal Activity. *Angew. Chem., Int. Ed.* **2011**, *50* (42), 9948−9952.

(13) Wiedner, E. S.; Chambers, M. B.; Pitman, C. L.; Bullock, R. M.; Miller, A. J. M.; Appel, A. M. Thermodynamic Hydricity of Transition Metal Hydrides. *Chem. Rev.* **2016**, *116* (15), 8655−8692.

(14) Brereton, K. R.; Smith, N. E.; Hazari, N.; Miller, A. J. M. Thermodynamic and kinetic hydricity of transition metal hydrides. *Chem. Soc. Rev.* **2020**, *49* (22), 7929−7948.

(15) Heimann, J. E.; Bernskoetter, W. H.; Hazari, N.; Mayer, James M. Acceleration of CO_2 insertion into metal hydrides: ligand, Lewis acid, and solvent effects on reaction kinetics. *Chem. Sci.* **2018**, *9* (32), 6629−6638.

(16) DuBois, D. L. Development of Molecular Electrocatalysts for Energy Storage. *Inorg. Chem.* **2014**, *53* (8), 3935−3960.

(17) Waldie, K. M.; Ostericher, A. L.; Reineke, M. H.; Sasayama, A. F.; Kubiak, C. P. Hydricity of Transition-Metal Hydrides: Thermodynamic Considerations for CO_2 Reduction. *ACS Catal.* **2018**, *8* (2), 1313−1324.

(18) Mathis, C. L.; Geary, J.; Ardon, Y.; Reese, M. S.; Philliber, M. A.; VanderLinden, R. T.; Saouma, C. T. Thermodynamic Analysis of Metal−Ligand Cooperativity of PNP Ru Complexes: Implications for CO_2 Hydrogenation to Methanol and Catalyst Inhibition. *J. Am. Chem. Soc.* **2019**, *141* (36), 14317−14328.

(19) Schlenker, K.; Casselman, L. K.; VanderLinden, R. T.; Saouma, C. T. Large changes in hydricity as a function of charge and not metal in (PNP)M−H (de)hydrogenation catalysts that undergo metal−ligand cooperativity. *Catal. Sci. Technol.* **2023**, *13* (5), 1358−1368.

(20) Matsubara, Y.; Fujita, E.; Doherty, M. D.; Muckerman, J. T.; Creutz, C. Thermodynamic and Kinetic Hydricity of Ruthenium(II) Hydride Complexes. *J. Am. Chem. Soc.* **2012**, *134* (38), 15743−15757.

(21) Hu, J.; Bruch, Q. J.; Miller, A. J. M. Temperature and Solvent Effects on H_2 Splitting and Hydricity: Ramifications on CO2 Hydrogenation by a Rhenium Pincer Catalyst. *J. Am. Chem. Soc.* **2021**, *143* (2), 945−954.

(22) Watson, L. A.; Coalter Iii, J. N.; Ozerov, O.; Pink, M.; Huffman, J. C.; Caulton, K. G. Amido/phosphine pincer hydrides of ruthenium. *New J. Chem.* **2003**, *27* (2), 263−273.

(23) Çelenligil-Çetin, R.; Watson, L. A.; Guo, C.; Foxman, B. M.; Ozerov, O. V. Decarbonylation of Acetone and Carbonate at a Pincer-Ligated Ru Center. *Organometallics* **2005**, *24* (2), 186−189.

(24) Askevold, B.; Khusniyarov, M. M.; Herdtweck, E.; Meyer, K.; Schneider, S. A Square-Planar Ruthenium(II) Complex with a Low-Spin Configuration. *Angew. Chem., Int. Ed.* **2010**, *49* (41), 7566−7569.

(25) Kessler, J. A.; Iluc, V. M. Ag(I) and Tl(I) Precursors as Transfer Agents of a Pyrrole-Based Pincer Ligand to Late Transition Metals. *Inorg. Chem.* **2014**, *53* (23), 12360−12371.

(26) Alberico, E.; Lennox, A. J. J.; Vogt, L. K.; Jiao, H.; Baumann, W.; Drexler, H.-J.; Nielsen, M.; Spannenberg, A.; Checinski, M. P.; Junge, H.; Beller, M. Unravelling the Mechanism of Basic Aqueous Methanol Dehydrogenation Catalyzed by Ru−PNP Pincer Complexes. *J. Am. Chem. Soc.* **2016**, *138* (45), 14890−14904.

(27) Rohmann, K.; Kothe, J.; Haenel, M. W.; Englert, U.; Hölscher, M.; Leitner, W. Hydrogenation of CO_2 to Formic Acid with a Highly Active Ruthenium Acriphos Complex in DMSO and DMSO/Water. *Angew. Chem., Int. Ed.* **2016**, *55* (31), 8966−8969.

(28) Kar, S.; Sen, R.; Kothandaraman, J.; Goeppert, A.; Chowdhury, R.; Munoz, S. B.; Haiges, R.; Prakash, G. K. S. Mechanistic Insights into Ruthenium-Pincer-Catalyzed Amine-Assisted Homogeneous Hydrogenation of CO_2 to Methanol. *J. Am. Chem. Soc.* **2019**, *141* (7), 3160−3170.

(29) Dub, P. A.; Gordon, J. C. The role of the metal-bound N−H functionality in Noyori-type molecular catalysts. *Nat. Rev. Chem.* **2018**, *2* (12), 396−408.

(30) Wang, Y.; Liu, S.; Yang, H.; Li, H.; Lan, Y.; Liu, Q. Structure, reactivity and catalytic properties of manganese-hydride amidate complexes. *Nat. Chem.* **2022**, *14* (11), 1233−1241.

(31) Anaby, A.; Schelwies, M.; Schwaben, J.; Rominger, F.; Hashmi, A. S. K.; Schaub, T. Study of Precatalyst Degradation Leading to the Discovery of a New Ru^0 Precatalyst for Hydrogenation and Dehydrogenation. *Organometallics* **2018**, *37* (13), 2193−2201.

(32) Choi, J.; Lee, Y. A Low-Spin Three-Coordinate Cobalt(I) Complex and Its Reactivity toward H_2 and Silane. *Angew. Chem., Int. Ed.* **2019**, *58* (21), 6938−6942.

(33) Yoo, C.; Lee, Y. A T-Shaped Nickel(I) Metalloradical Species. *Angew. Chem., Int. Ed.* **2017**, *56* (32), 9502−9506.

(34) Kim, Y.-E.; Kim, J.; Lee, Y. Formation of a nickel carbon dioxide adduct and its transformation mediated by a Lewis acid. *Chem. Commun.* **2014**, *50* (78), 11458−11461.

(35) Yoo, C.; Lee, Y. Formation of a tetranickel octacarbonyl cluster from the CO_2 reaction of a zero-valent nickel monocarbonyl species. *Inorg. Chem. Front.* **2016**, *3* (6), 849−855.

(36) Yoo, C.; Lee, Y. Carbon dioxide binding at a Ni/Fe center: synthesis and characterization of Ni(η^1-CO_2-κC) and Ni-μ-CO_2-κC:κ^2O,O′-Fe. *Chem. Sci.* **2017**, *8* (1), 600−605.

(37) Yoo, C.; Kim, Y.-E.; Lee, Y. Selective Transformation of CO_2 to CO at a Single Nickel Center. *Acc. Chem. Res.* **2018**, *51* (5), 1144−1152.

(38) Sahoo, D.; Yoo, C.; Lee, Y. Direct CO_2 Addition to a Ni(0)−CO Species Allows the Selective Generation of a Nickel(II) Carboxylate with Expulsion of CO. *J. Am. Chem. Soc.* **2018**, *140* (6), 2179−2185.

(39) Min, S.; Choi, J.; Yoo, C.; Graham, P. M.; Lee, Y. Ni(0)-promoted activation of C_{sp2}−H and C_{sp2}−O bonds. *Chem. Sci.* **2021**, *12* (29), 9983−9990.

(40) Lee, K.; Choi, J.; Graham, P. M.; Lee, Y. Binding of carbon monoxide at a single nickel center and its oxidative reactivity toward CO and O. *Bull. Korean Chem. Soc.* **2022**, *43* (2), 222−226.

(41) Park, S.; Lee, K.; Padmanaban, S.; Lee, Y. Small Molecule Activation at the ^{acri}PNP Pincer-Supported Nickel Sites. *Acc. Chem. Res.* **2024**, *57* (21), 3093−3101.

(42) Pingen, D.; Choi, J.-H.; Allen, H.; Murray, G.; Ganji, P.; van Leeuwen, P. W. N. M.; Prechtl, M. H. G.; Vogt, D. Amide versus amine ligand paradigm in the direct amination of alcohols with Ru-PNP complexes. *Catal. Sci. Technol.* **2018**, *8* (15), 3969−3976.

(43) Tindall, D. J.; Menche, M.; Schelwies, M.; Paciello, R. A.; Schäfer, A.; Comba, P.; Rominger, F.; Hashmi, A. S. K.; Schaub, T. Ru0 or RuII: A Study on Stabilizing the "Activated" Form of Ru-PNP Complexes with Additional Phosphine Ligands in Alcohol Dehydrogenation and Ester Hydrogenation. *Inorg. Chem.* **2020**, *59* (7), 5099−5115.

(44) Schmeier, T. J.; Dobereiner, G. E.; Crabtree, R. H.; Hazari, N. Secondary Coordination Sphere Interactions Facilitate the Insertion Step in an Iridium(III) CO_2 Reduction Catalyst. *J. Am. Chem. Soc.* **2011**, *133* (24), 9274−9277.

(45) Heimann, J. E.; Bernskoetter, W. H.; Hazari, N. Understanding the Individual and Combined Effects of Solvent and Lewis Acid on CO_2 Insertion into a Metal Hydride. *J. Am. Chem. Soc.* **2019**, *141* (26), 10520−10529.

(46) Stepowska, E.; Jiang, H.; Song, D. Reversible H_2 splitting between Ru(ii) and a remote carbanion in a zwitterionic compound. *Chem. Commun.* **2010**, *46* (4), 556−558.

(47) Tossaint, A. S.; Rebreyend, C.; Sinha, V.; Weber, M.; Canossa, S.; Pidko, E. A.; Filonenko, G. A. Two step activation of Ru-PN_3P pincer catalysts for CO_2 hydrogenation. *Catal. Sci. Technol.* **2022**, *12* (9), 2972−2977.

(48) Padmanaban, S.; Chun, J.; Lee, Y.; Cho, K.-B.; Choi, J.; Lee, Y. Nitrate Upcycling Mediated by Organonickel Catalysis. *Angew. Chem., Int. Ed.* **2024**, No. e202408457.

(49) Curley, J. B.; Hert, C.; Bernskoetter, W. H.; Hazari, N.; Mercado, B. Q. Control of Catalyst Isomers Using an N-Phenyl-Substituted RN($CH_2CH_2P^iPr_2$)$_2$ Pincer Ligand in CO_2 Hydrogenation and Formic Acid Dehydrogenation. *Inorg. Chem.* **2022**, *61* (1), 643−656.

(50) Saame, J.; Rodima, T.; Tshepelevitsh, S.; Kütt, A.; Kaljurand, I.; Haljasorg, T.; Koppel, I. A.; Leito, I. Experimental Basicities of Superbasic Phosphonium Ylides and Phosphazenes. *J. Org. Chem.* **2016**, *81* (17), 7349−7361.

(51) Fong, H.; Peters, J. C. Hydricity of an Fe−H Species and Catalytic CO_2 Hydrogenation. *Inorg. Chem.* **2015**, *54* (11), 5124−5135.

(52) Vollmer, M. V.; Ye, J.; Linehan, J. C.; Graziano, B. J.; Preston, A.; Wiedner, E. S.; Lu, C. C. Cobalt-Group 13 Complexes Catalyze CO_2 Hydrogenation via a Co(−I)/Co(I) Redox Cycle. *ACS Catal.* **2020**, *10* (4), 2459−2470.

(53) Ciancanelli, R.; Noll, B. C.; DuBois, D. L.; DuBois, M. R. Comprehensive Thermodynamic Characterization of the Metal−Hydrogen Bond in a Series of Cobalt-Hydride Complexes. *J. Am. Chem. Soc.* **2002**, *124* (12), 2984−2992.

(54) Roberts, J. A. S.; Appel, A. M.; DuBois, D. L.; Bullock, R. M. Comprehensive Thermochemistry of W−H Bonding in the Metal Hydrides CpW(CO)$_2$(IMes)H, [CpW(CO)$_2$(IMes)H]$^{•+}$, and [CpW-(CO)$_2$(IMes)(H)$_2$]$^+$. Influence of an N-Heterocyclic Carbene Ligand on Metal Hydride Bond Energies. *J. Am. Chem. Soc.* **2011**, *133* (37), 14604−14613.

(55) Wilson, A. D.; Miller, A. J. M.; DuBois, D. L.; Labinger, J. A.; Bercaw, J. E. Thermodynamic Studies of [H_2Rh(diphosphine)$_2$]$^+$ and [HRh(diphosphine)$_2$(CH$_3$CN)]$^{2+}$ Complexes in Acetonitrile. *Inorg. Chem.* **2010**, *49* (8), 3918−3926.

(56) Curley, J. B.; Smith, N. E.; Bernskoetter, W. H.; Ertem, M. Z.; Hazari, N.; Mercado, B. Q.; Townsend, T. M.; Wang, X. Understanding the Reactivity and Decomposition of a Highly Active Iron Pincer Catalyst for Hydrogenation and Dehydrogenation Reactions. *ACS Catal.* **2021**, *11* (16), 10631−10646.

(57) Prat, J. R.; Cammarota, R. C.; Graziano, B. J.; Moore, J. T.; Lu, C. C. Toggling the Z-type interaction off-on in nickel-boron dihydrogen and anionic hydride complexes. *Chem. Commun.* **2022**, *58* (63), 8798−8801.

(58) Crabtree, R. H. Dihydrogen Complexation. *Chem. Rev.* **2016**, *116* (15), 8750−8769.

(59) Kubas, G. J. Fundamentals of H_2 Binding and Reactivity on Transition Metals Underlying Hydrogenase Function and H2 Production and Storage. *Chem. Rev.* **2007**, *107* (10), 4152−4205.

(60) Alós, J.; Bolaño, T.; Esteruelas, M. A.; Oliván, M.; Oñate, E.; Valencia, M. POP−Pincer Ruthenium Complexes: d^6 Counterparts of Osmium d^4 Species. *Inorg. Chem.* **2014**, *53* (2), 1195−1209.

(61) Choi, J.-H.; Schloerer, N. E.; Berger, J.; Prechtl, M. H. G. Synthesis and characterisation of ruthenium dihydrogen complexes and their reactivity towards B−H bonds. *Dalton Trans.* **2014**, *43* (1), 290−299.

(62) Prechtl, M. H. G.; Ben-David, Y.; Ben-David, Y.; Giunta, D.; Busch, S.; Taniguchi, Y.; Wisniewski, W.; Görls, H.; Mynott, R. J.; Theyssen, N.; Milstein, D. Synthesis and Characterisation of Nonclassical Ruthenium Hydride Complexes Containing Chelating Bidentate and Tridentate Phosphine Ligands. *Chem. - Eur. J.* **2007**, *13* (5), 1539−1546.

(63) Wang, W.-H.; Himeda, Y.; Muckerman, J. T.; Manbeck, G. F.; Fujita, E. CO_2 Hydrogenation to Formate and Methanol as an Alternative to Photo- and Electrochemical CO_2 Reduction. *Chem. Rev.* **2015**, *115* (23), 12936−12973.

(64) Kothandaraman, J.; Czaun, M.; Goeppert, A.; Haiges, R.; Jones, J.-P.; May, R. B.; Prakash, G. K. S.; Olah, G. A. Amine-Free Reversible Hydrogen Storage in Formate Salts Catalyzed by Ruthenium Pincer Complex without pH Control or Solvent Change. *ChemSusChem* **2015**, *8* (8), 1442−1451.

(65) Sheldrick, G. M. SHELXT - Integrated space-group and crystal-structure determination. *Acta Crystallogr., Sect. A: Found. Adv.* **2015**, *71* (1), 3−8.

(66) Sheldrick, G. M. Crystal structure refinement with SHELXL. *Acta Crystallogr., Sect. C: Struct. Chem.* **2015**, *71* (1), 3−8.

(67) Becke, A. D. Density-functional thermochemistry. III. The role of exact exchange. *J. Chem. Phys.* **1993**, *98* (7), 5648−5652.

(68) Weigend, F.; Ahlrichs, R. Balanced basis sets of split valence, triple zeta valence and quadruple zeta valence quality for H to Rn: Design and assessment of accuracy. *Phys. Chem. Chem. Phys.* **2005**, *7* (18), 3297−3305.

(69) Fox, M. J.; Trucks, G. W.; Schlegel, H. B.; Scuseria, G. E.; Robb, M. A.; Cheeseman, J. R.; Scalmani, G.; Barone, V.; Petersson, G. A.; Nakatsuji, H.; Li, X.; Caricato, M.; Marenich, A. V.; Bloino, J.; Janesko, B. G.; Gomperts, R.; Mennucci, B.; Hratchian, H. P.; Ortiz, J. V.; Izmaylov, A. F.; Sonnenberg, J. L.; Williams-Young, D.; Ding, F.; Lipparini, F.; Egidi, F.; Goings, J.; Peng, B.; Petrone, A.; Henderson, T.; Ranasinghe, D.; Zakrzewski, V. G.; Gao, J.; Rega, N.; Zheng, G.; Liang, W.; Hada, M.; Ehara, M.; Toyota, K.; Fukuda, R.; Hasegawa, J.; Ishida, M.; Nakajima, T.; Honda, Y.; Kitao, O.; Nakai, H.; Vreven, T.; Throssell, K.; Montgomery, J. A., Jr.; Peralta, J. E.; Ogliaro, F.;

Bearpark, M. J.; Heyd, J. J.; Brothers, E. N.; Kudin, K. N.; Staroverov, V. N.; Keith, T. A.; Kobayashi, R.; Normand, J.; Raghavachari, K.; Rendell, A. P.; Burant, J. C.; Iyengar, S. S.; Tomasi, J.; Cossi, M.; Millam, J. M.; Klene, M.; Adamo, C.; Cammi, R.; Ochterski, J. W.; Martin, R. L.; Morokuma, K.; Farkas, O.; Foresman, J. B.; Fox, D. J. *Gaussian 16*, revision 01, B; Gaussian, Inc.: Wallingford CT, 2016.

(70) Zhao, Y.; Truhlar, D. G. The M06 suite of density functionals for main group thermochemistry, thermochemical kinetics, non-covalent interactions, excited states, and transition elements: two new functionals and systematic testing of four M06-class functionals and 12 other functionals. *Theor. Chem. Acc.* **2008**, *120* (1), 215−241.

(71) Barone, V.; Cossi, M. Quantum Calculation of Molecular Energies and Energy Gradients in Solution by a Conductor Solvent Model. *J. Phys. Chem. A* **1998**, *102* (11), 1995−2001.

(72) Cossi, M.; Rega, N.; Scalmani, G.; Barone, V. Energies, structures, and electronic properties of molecules in solution with the C-PCM solvation model. *J. Comput. Chem.* **2003**, *24* (6), 669−681.